# ER-located PIN5 transporter generates potent auxin sinks driven by the IAA decarboxylation pathway

Milada Čovanová, Karel Müller, Nikoleta Klierová, Nayyer Abdollahi Sisi, Petr Skůpa, Ondřej Smetana, Petre Ivanov Dobrev, Kamil Růžička*, Jan Petrášek*

Institute of Experimental Botany CAS, Rozvojová 263, 165 02 Prague 6, Czech Republic
*For correspondence (e-mail kamil.ruzicka@ueb.cas.cz, petrasek@ueb.cas.cz)

## ABSTRACT

Auxin is an essential and well-investigated regulator of plant development. Still, many aspects determining its (sub-)cellular distribution, as well as its metabolic turnover, are obscure. PIN5 is a transporter that resides on the endoplasmic reticulum and is presumed to influence internal auxin homeostasis by direct sequestration and subsequent degradation. Due to its distinct expression pattern and incomplete metabolomics analyses, the exact role of PIN5 protein and the identity of downstream auxin degradation products show significant gaps. To this end, we utilized morphologically homogeneous tobacco BY-2 cell cultures. We show that the expression of *Arabidopsis thaliana AtPIN5* in the BY-2 system phenocopies so-called auxin starvation defects. Moreover, we reveal that the activity of *At*PIN5 leads, in extreme cases, to the broad range of processes accompanying programmed cell death (PCD). Notably, based on the recently updated knowledge on auxin metabolism, we also show that a significant part of auxin metabolites downstream of the *At*PIN5 activity are part of the re-emerging auxin decarboxylation pathway. Taking together, we report the direct induction of PCD by auxin stimulus and propose the physiological framework of the auxin decarboxylation route.

## INTRODUCTION

The phytohormone auxin, or indole-3-acetic acid (IAA), is vital for plant growth and development. The pattern formation at the level of individual tissues and organs is achieved

by the formation of local auxin maxima or minima, orchestrated by the cell-to-cell transport of IAA (Weijers *et al.*, 2021). Among the mediators of auxin flow emerge the transporters of the PIN-formed (PIN) family. Showing a remarkable asymmetrical distribution on the plasma membrane (PM), they coordinate auxin fluxes across the tissues, thereby controlling the downstream developmental programs (Adamowski & Friml, 2015). Recent crystallographic studies of the PIN transporters (Su *et al.*, 2022; Ung *et al.*, 2022; Yang *et al.*, 2022) brought compelling insights into the molecular mechanism of auxin transport over the membrane (Andersen *et al.*, 2023; Ung *et al.*, 2023a,b).

Besides the well-investigated auxin fluxes between cells, mediated by the PM-located PINs, another group of PIN proteins residing at the endoplasmic reticulum (ER) has been described. The so-called ER-PINs regulate internal auxin levels by conveying auxin into the ER lumen for subsequent metabolization (Mravec *et al.*, 2009; Ding *et al.*, 2012). The metabolic products downstream of the ER-located PIN activity have been examined several times and with various degrees of consistency (Mravec *et al.*, 2009; Ding *et al.*, 2012; Abdollahi Sisi & Růžička, 2020). In addition, the pathways accompanying the IAA breakdown have recently undergone revision (Müller *et al.*, 2021; Hayashi *et al.*, 2021; Dobrev *et al.*, 2023), highlighting the IAA decarboxylation as another relevant auxin degradation route (Bandurski *et al.*, 1995; Dobrev *et al.*, 2023). Thus, many aspects of the IAA homeostasis controlled by ER-PINs remain unclear (Abdollahi Sisi & Růžička, 2020; Ung *et al.*, 2023a).

The connection between auxin and programmed cell death (PCD) has been repeatedly proposed (Kacprzyk *et al.*, 2022). It was shown that auxin pulses produced from the cells undergoing PCD in the outermost layers of the root cap are required for priming lateral root primordia in the primary root meristem (Xuan *et al.*, 2015, 2016). It was also revealed that auxin can suppress certain instances of PCD (Kerchev *et al.*, 2013). It has even been hypothesized that auxin is a product of tryptophan degradation occurring in defunct cells (Sheldrake, 2021). However, the authentic effect of auxin activity to trigger PCD has never been presented.

Cell-suspension cultures have proved to be an excellent model system, which enables studying the effects of growth substances directly and in a homogeneous manner (Petrášek & Zazímalová, 2006; Petrasek *et al.*, 2006). Here, we explore the impact of conditional expression of the well-characterized ER-located *Arabidopsis thaliana At*PIN5 (Mravec *et al.*,

2009) in the BY-2 tobacco suspension cultures. We comprehensively analyze the immediate IAA metabolites downstream of PIN5 activity and reveal the remarkably elevated presence of products of the IAA decarboxylation pathway (Dobrev *et al.*, 2023). We also describe the corresponding phenotypic consequences, including the extreme instances of PCD.

## RESULTS

### Auxin response is required for controlling cell expansion and division rates of the BY-2 tobacco cell cultures

The growth and proliferation of tobacco BY-2 cells depends on the exogenous supply of auxin to the media. Its absence is generally characterized by enhanced cell elongation and lowered cell division, termed collectively as symptoms of auxin starvation (Winicur *et al.*, 1998). Our previous work has revealed that interfering with auxin transport leads to similar morphological defects (Mravec *et al.*, 2008; Müller *et al.*, 2019). Indeed, the induction of the transgene encoding a PM-located *Arabidopsis thaliana At*PIN7 auxin carrier enhances cell elongation (Figure 1a) and division arrest (Figures 1b and S1a), consistent with that occurring on the auxin-free medium (Figure S1b; Mravec *et al.*, 2008; Müller *et al.*, 2019). We observed similar auxin-deficient phenotypes by interfering with auxin signaling by the inducible expression of the stabilized version of the auxin signaling repressor *At*IAA17, *At*axr3-1 (Leyser *et al.*, 1996; Knox *et al.*, 2003; Figures 1c-e). We were also able to pharmacologically reduce cell proliferation by the dose-dependent application of IAA antagonist PEO-IAA, which competitively binds the TIR1/AFBs auxin receptors (Nishimura *et al.*, 2009; Figure 1f). This indicates that the auxin starvation phenotypes are dependent on the TIR1/AFB signaling, in addition to the availability of auxin in the cells.

### Inducible expression of *At*PIN5 leads to defects corresponding to the symptoms of auxin starvation in BY-2 cells

Next, to study the impact of internal auxin fluxes on the cell culture phenotypes, we expressed in the BY-2 cells the characterized *Arabidopsis thaliana* gene *AtPIN5* (Mravec *et al.*, 2009; Abdollahi Sisi & Růžička, 2020). We employed two independent transcription inducible systems, XVE (Zuo *et al.*, 2000; Petrasek *et al.*, 2006) and GVG (Aoyama & Chua, 1997; Mravec *et al.*, 2008), triggering the expression at the beginning of the subculture

interval. Normally, under control conditions, on the third day of the subculture cycle, the cultures turn into the exponential growth phase manifested by intensive cell divisions, reflective of cell files consisting of short cells (Figures 2a and S2a). Upon the induction of the *At*PIN5 transgene, the cells became remarkably expanded (Figures 2a and S2a, 2b and S2b), and their cell division reduced (Figures 2c and S2c), akin to the auxin starvation phenotypes (Figures 1 and S1). We also co-transformed the cells carrying the inducible *AtPIN5-GFP* construct with the transcriptionally-dependent auxin reporter *DR5::RFP* (Barbez *et al.*, 2013). Although the intensity of the induced GFP signal in individual cells varied across the population, the simultaneous presence of AtPIN5-GFP was generally able to lower the *DR5::RFP* signal (Figures 2d, e). This indicates that the *At*PIN5 activity is capable of changing the internal availability of auxin to control the growth and expansion of the BY-2 cells.

**IAA enhances the symptoms of *At*PIN5-induced auxin starvation**

The dependence of the BY-2 tissue cultures on the addition of the synthetic auxin (2,4-dichlorophenoxyacetic acid or 2,4-D) to the media is ascribed to the low levels of endogenous IAA in the cells, caused by its native metabolization (Simon *et al.*, 2013; Seifertová *et al.*, 2014; Müller *et al.*, 2021). Accordingly, the cultivation in the presence of IAA also leads to auxin starvation phenotypes (Simon *et al.*, 2013; Figure 3a). To test the role of internal auxin fluxes under conditions where only native auxin is present, we cultivated the cells expressing *AtPIN5* under the supply of IAA, too. The control lines proliferated less intensively and resembled the auxin-starved ones. Surprisingly, the induction of *At*PIN5 led to even stronger auxin starvation phenotypes (Figures 3b, c). Thus, it seems that the PIN5-like transporters can even enhance rapid IAA turnover in BY-2 cells.

To follow the original idea and to compensate for the fast IAA metabolization more efficiently, we were continuously adding IAA to the media every 12 h during the cultivation. We observed a rescue of the cell proliferation in the control cells; they displayed no apparent signs of auxin starvation (Figures 3d and 3e). Strikingly, though, the *AtPIN5* induction caused strong auxin starvation phenotypes (Figures 3d and 3e). Under these conditions, PIN5-GFP was present on ER as in cells cultivated on 2,4-D, also reporting the absence of remarkable morphological changes of this compartment (Figure S3). This further underlines that PIN5 is able to generate a potent intracellular IAA sink.

ER-PINs specifically transport both IAA and 2,4-D (Ung *et al.*, 2022). Hence, we measured the cellular accumulation of radioactively labeled [$^3$H]-IAA and [$^3$H]-2,4-D following the induction of *AtPIN5*. The lines showed a strong cellular uptake of [$^3$H]-IAA (Figure 2f). Interestingly, we observed no change in the *At*PIN5-mediated [$^3$H]-2,4-D accumulation (Figure 2g). Altogether, our data suggest that *At*PIN5 efficiently channels IAA from the cytosol to be delivered to likely highly active metabolic enzymes inside the ER lumen.

**Induction of *AtPIN5* promotes programmed cell death**

To validate whether the strong auxin withdrawal from the cytosol by *At*PIN5 corresponds to a native downstream process, we analyzed the viability of the cells examined. As revealed by the trypan blue exclusion test (van Wees, 2008), we observed an increased ratio of cells showing a dye-positive cytoplasm shrinkage as a sign of decreased cell viability following the *At*PIN5 induction (Figures 4a, b and S4a, b). Moreover, the internal trypan blue staining was even more apparent in the cells cultured on IAA (Figures 4a, b). This shows that the PIN5-mediated funneling of auxin from the cytosol can indeed lead to increased mortality of BY-2 cells.

Further, we analyzed the global transcriptional changes downstream of the *At*PIN5 activity to hint at the possible relevant physiological processes related to auxin starvation and lower cell viability. Indeed, using the PANTHER overrepresentation test (Mi *et al.*, 2019), we found a remarkable overlap with the previously published transcriptional profiles from the BY-2 cells cultured in the auxin-free medium (Müller et al., 2021; Figures 4c and S4c, d). This included pronounced changes in the expression of stress-related genes, particularly peroxidases (Table S1). We further examined the transcriptional response exclusively linked with the *At*PIN5 expression (Table S2), revealing a single enriched gene ontology term (GO:0000041) supported by 6 individual transcripts coding for transporters of transition metals (Peñarrubia *et al.*, 2015). This suggests that the auxin starvation is associated with the enhanced expression of the stress-related peroxidases and that the *AtPIN5* expression leads to the enhanced metal ion transport, presumably activating the response preceding the cell death.

The increased expression of peroxidases following the *AtPIN5* induction suggests elevated activity of produced reactive oxygen species (ROS). The role of auxin has been implicated in the crosstalk with ROS homeostasis (Tognetti *et al.*, 2012; Chen *et al.*, 2014b). Hence, we

utilized a sensor carboxy-2',7'-dichloro-dihydro-fluorescein diacetate (H2DCFDA), which indicates the intracellular presence of various ROS, including $H_2O_2$ (Akter *et al.*, 2021). Indeed, upon induction of *AtPIN5*, the cells displayed significantly increased H2DCFDA fluorescence, corroborating the enhanced ROS activity (Figures 4d, e, and S4e). PIN5 was previously shown to be a part of ER stress adaptive mechanisms (Chen *et al.*, 2014a). Although we did not notice that the repeated additions of IAA into the media would influence the ER localization of *At*PIN5-GFP or lead to remarkable changes in the overall ER structural pattern (Figures 2d and S3), pathways involving ROS production and ER stress are often preceding PCD (Petrov *et al.*, 2015). Hence, this further highlights that the lower viability of the *At*PIN5-GFP cells accompanied by ROS can be perhaps ascribed to the initiation of processes related to PCD.

Among the main features of PCD is vacuolar leakage and subsequent acidification of cytoplasm (Valandro *et al.*, 2020). To this end, we utilized 2',7'-Bis-(2-carboxyethyl)-5-(and-6)-carboxyfluorescein acetoxymethyl ester (BCECF/AM), a fluorescent dye used for analyzing lowered cytosolic pH as a result of disrupted vacuolar integrity (Scheuring *et al.*, 2015). Under control conditions, the cells contained several smaller vacuoles. The induction of *At*PIN5 led to the enlargement of central vacuoles, their occasional collapse and acidification of the whole cytoplasm and nucleus (Figures 4f, g). Finally, we tested the nuclear DNA fragmentation, a hallmark of PCD, using terminal deoxynucleotidyl transferase-mediated dUTP nick-end labeling (TUNEL) (Tripathi *et al.*, 2017). The expression of *AtPIN5* (Figures 4h, i, and S4f) resulted in an increased number of TUNEL-stained nuclei, highlighting that DNA fragmentation takes part in the signaling cascade downstream of the rapid depletion of auxin in the cytoplasm. Taken together, we conclude that the decreased cell viability associated with PCD, different from uncontrolled stress-related necrotic processes (Van Durme & Nowack, 2016), is another hallmark of PIN5-triggered auxin starvation.

**The activity of *At*PIN5 stimulates auxin degradation by the IAA decarboxylation pathway**

To get insights into how the ER-mediated IAA conversion affects internal auxin homeostasis in light of recent findings (Müller *et al.*, 2021; Hayashi *et al.*, 2021; Dobrev *et al.*, 2023; Figure 5a), we have tracked the expanded list of IAA metabolites by liquid chromatography-mass spectrometry (LC-MS) resulting from the *AtPIN5* induction. At the time point of adding IAA into media ($t_0$), its degradation products were barely detectable

and their amounts showed negligible differences between the mock and chemical inducer-treated cells (Figure S5a). 2 hours later, we observed that IAA was converted predominantly to amino-acid conjugates of IAA (Figure 5b; see also Seifertová *et al.*, 2014; Müller *et al.*, 2021; Dobrev *et al.*, 2023). The induction of *AtPIN5* usually led to a further increase in IAA conversion in this experimental setup (Figures 5b and S5b). These measurements illustrate rapid catabolism of IAA in BY-2 cells and evidence that the majority of detected metabolic compounds indeed originate from the supplied IAA.

Next, we quantified the IAA breakdown in the cells cultivated in a media supplied with IAA every 12 hours from the beginning of the subcultivation interval. 2 hours after addition, IAA was converted in the control lines into its conjugates as well (Figure 5c). Surprisingly, the prior induction of *AtPIN5* dramatically reduced the internal IAA levels to close to trace amounts. Although we were also able to detect the activity of the common oxidative IAA degradation pathway, we found remarkably increased conversion towards IAA decarboxylation in these lines (Figure 5c), as documented by the elevated levels of ascorbigen (Abg) and dihydroascorbigen (DiHAbg) (Dobrev *et al.*, 2023; Figure 5c). We therefore conclude that the PIN5-mediated auxin sinks are at least partially accompanied by the increased activity of the auxin decarboxylation pathway.

**The exogenous application of I3C leads to symptoms of cell death in BY-2 cells**

It has been proposed earlier that indole-3-carbinol (I3C), an unstable immediate IAA decarboxylation product and precursor of Abg (Figure 5a) (Hrnčiřík *et al.*, 1998; Chhajed *et al.*, 2020; Dobrev *et al.*, 2023), can function as an auxin antagonist and can stimulate vacuolar disintegration and processes related to autophagy in *Arabidopsis* as a result of defense reaction (Katz *et al.*, 2015; Katz & Chamovitz, 2017). We therefore incubated the cells with I3C to relate its role to the PIN5-mediated programmed cell death in the BY-2 cultures. Despite the default presence of 2,4-D in the media, I3C treatment affected the cell expansion and proliferation rates (Figure 6a, b), and also caused a significant decrease in their viability (Figure 6c, d). Taken together, ER represents a powerful auxin sink for the degradation of endogenous IAA, metabolized by the IAA decarboxylation pathway that appears to be capable of triggering PCD.

## DISCUSSION

### A possible mechanism underlying PIN5-mediated auxin sinks

The classical concept of polar auxin transport has premised the existence of efflux carriers asymmetrically localized at PM as the central prerequisite for the directional flow of IAA (Rubery & Sheldrake, 1974; Raven, 1975). Later, the PIN auxin transporters were discovered, matching henceforth the proposed attributes of the main IAA carriers (Gälweiler *et al.*, 1998; Petrasek *et al.*, 2006). ER-located PINs were found subsequently, and the relevant works highlighted their capability to influence internal auxin homeostasis (Mravec *et al.*, 2009; Ding *et al.*, 2012; Abdollahi Sisi & Růžička, 2020). Further, the detailed crystallographic studies evidenced that the transporting mechanism employed by both PM and ER-located PINs is identical (Su *et al.*, 2022; Ung *et al.*, 2022; Yang *et al.*, 2022).

Yet, many aspects of the PIN-mediated transport remain obscure. Compelling arguments supported by the structural models suggest that IAA is transported from the cytosol against concentration gradients at the expense of membrane potential (Su *et al.*, 2022; Ung *et al.*, 2022, 2023a,b; Yang *et al.*, 2022; Andersen *et al.*, 2023). Indeed, in the root apical meristem, PM-located PINs concentrate auxin in the uttermost root tip (Adamowski & Friml, 2015). They also establish and maintain auxin maxima, determining the position of flower primordia in the shoot apical meristem in an equivalent manner (Reinhardt *et al.*, 2003). In contrast, the canalization hypothesis proposes that auxin is funneled away from the site of its external application, i.e., source, towards the sink in the established vascular tissue determining the connective vascular strands (Mitchison, 1980; Sachs, 1991; Ravichandran *et al.*, 2020). Similarly, the root or hypocotyl tropic reactions depend on the transport outwards from the tissue with higher auxin concentration (Friml *et al.*, 2002; Ottenschläger *et al.*, 2003; Rakusová *et al.*, 2011; Band *et al.*, 2012). The expression of PIN5 proteins leads to a remarkable auxin deficiency in BY-2 cells. In the conditions when 2,4-D does not interfere with the internal IAA fluxes (Figure 5b), the excess of IAA leads to even enhanced PIN5-mediated auxin degradation rates. Hence, in this system, the PIN5-like auxin transporters likely operate in the source-sink mode, too, perhaps by the mechanism of facilitated diffusion, as earlier presumed for auxin canalization (Mitchison, 1980; Rolland-Lagan & Prusinkiewicz, 2005).

**Auxin metabolization as a trigger for PCD**

Along with the auxin-dependent processes, PCD is an inherent part of plant development. The connections between auxin and PCD pathways have been proposed, but mostly indirectly (reviewed in Van Durme & Nowack, 2016; Sheldrake, 2021; Kacprzyk *et al.*, 2022). A chemical screen performed by Kerchev *et al.* (2013) revealed that the $H_2O_2$-dependent cell death caused by defective photorespiration can be reverted by both synthetic auxins and IAA. Auxin has been demonstrated as a central regulator of xylem patterning, where PCD gives rise to conductive vessels (Escamez & Tuominen, 2014; Ruzicka *et al.*, 2015); direct transdifferentiation of the tissue cultures into xylem vessels can also be induced by external cues (Fukuda & Komamine, 1980; Kubo *et al.*, 2005; Ruzicka *et al.*, 2015). In addition, various stages of lateral root development are determined by auxin activity in parallel to PCD (Casimiro *et al.*, 2001; Benková *et al.*, 2003; Swarup *et al.*, 2008; Escamez *et al.*, 2020). Auxin serves as a signal produced by the cells undergoing PCD in the root cap to prime the prospective lateral roots in the primary root meristem (Xuan *et al.*, 2015, 2016). Ultimately, Di Mambro et al. (2019) presented the model that the activity of *PIN5* in the lateral root cap affects root meristem size, but the direct influence of PIN5 on PCD in the lateral root cap has not been investigated.

We show that the ER-mediated auxin sinks can trigger PCD in BY-2 cultures. We have not noticed any cells resembling forming xylem vessels following the *AtPIN5* induction. Instead, we observed phenotypes associated with common PCD and present lines of evidence that they are linked with the auxin decarboxylation activity. I3C is among native metabolites of glucosinolates, a diverse group of small compounds produced predominantly in *Brassicales*, functioning as agent in the insect defense (Fahey *et al.*, 2001). It is also a product of auxin decarboxylation pathway in a multitude of the (non-)*Brassicales* plant species (Bandurski *et al.*, 1995; Kerk *et al.*, 2000; Dobrev *et al.*, 2023). I3C can induce some symptoms of PCD in *Arabidopsis*, in a competitive manner to IAA (Katz *et al.*, 2015; Katz & Chamovitz, 2017). Hence, our data suggest that the two pathways determining PCD overlap and share an unexpectedly common and likely evolutionally conserved functional output.

### IAA decarboxylation pathway downstream of PIN5-mediated auxin sequestration

PIN5 transports auxin into the ER in order to promote auxin degradation (Mravec *et al.*, 2009; Ung *et al.*, 2023a). The levels of IAA-aspartate and IAA-glutamate conjugates are elevated following *At*PIN5 overexpression (Mravec *et al.*, 2009). Paradoxically, the GRETCHEN HAGEN (GH3) enzymes catalyzing the IAA conjugation are generally seen in the cytoplasm (Ludwig-Müller *et al.*, 2009; Ostrowski *et al.*, 2014; Di Mambro *et al.*, 2019; Abdollahi Sisi & Růžička, 2020; Zou *et al.*, 2022). We have recently uncovered a new level of complexity of the IAA metabolome. Among known IAA breakdown routes emerges the auxin decarboxylation pathway, which includes Abg and DiHAbg. Even if occurring across angiosperms, the purpose of auxin decarboxylation is unknown (Dobrev *et al.*, 2023). Strikingly, we found that the relevant metabolic compounds are related to increased AtPIN5 activity. Hence, we conclude that IAA decarboxylation is the main and potent auxin degradation pathway downstream of PIN5.

## EXPERIMENTAL PROCEDURES

### Plant material, growth conditions and treatments

The tobacco cell lines BY-2 (*Nicotiana tabacum* L., cv. Bright Yellow-2; Nagata *et al.*, 1992) were standardly cultivated in a liquid medium supplemented with 1 µM 2,4-D as described in Petrasek *et al.* (2006) unless stated otherwise. The transformation of cell lines, RT-qPCR validation of the transgene expression, and cell line maintenance were done as described earlier (Petrasek *et al.*, 2006; Müller *et al.*, 2021). For all experiments, the cells in the exponential growth stage were used, typically 4-d-old, unless specified otherwise.

The expression of the *AtPIN7, AtPIN5* and *Ataxr3-1* genes was induced by 1 µM dexamethasone (30 mM stock solution, GVG lines) or 3 µM β-estradiol (30 mM stock solution, XVE lines) at the beginning of the subculture interval. In addition, 2-(1H-indol-3-yl)-4-oxo-4-phenyl-butyric acid (PEO-IAA; OlChemIm, Olomouc, Czech Republic, 10 mM stock solution) and indole-3-carbinol (I3C; Sigma-Aldrich, Merck KGaA, Darmstadt, Germany, 160 mM stock solution) were used. The respective compounds were applied to the cells at the

beginning of the subculture interval, and the corresponding amount of the solvent (DMSO) was added to the controls.

**Molecular transgenic work**

The dexamethasone-inducible gene constructs, *35S>>GVG::AtPIN5* and *35S>>GVG::AtPIN7*, including the corresponding cell cultures, have been described earlier (Petrasek *et al.*, 2006; Mravec *et al.*, 2009). For creating *G10-90>>XVE::AtPIN5*, the corresponding *AtPIN5* open reading frame was cloned with the Gateway system (Invitrogen, Thermo Fisher Scientific, Waltham, MA, USA) into the pMDC7 vector (Curtis & Grossniklaus, 2003). The respective Gateway entry clones were generated either by the amplification of wild-type DNA template or that originating from the *PIN5-GFP*$^{MGS}$ plants (Verna *et al.*, 2015) (primer sequences AAAAAGCAGGCTATATGATAAATTGTGGAGAT and AAGAAAGCTGGGTTTCAATGAATAAACTCC). The *XVE::AtPIN5-GFP/DR5::RFP* cell line was obtained by transformation of the *XVE::AtPIN5-GFP* line with the *DR5::RFP* construct (Barbez *et al.*, 2013). The *G10-90>>XVE::Ataxr3-1* line was generated by the transformation of BY-2 cells with the construct kindly provided by Jiří Friml.

**Microscopy and image analysis**

Nomarski differential interference contrast (DIC) microscopy was performed with the Nikon Eclipse E600 microscope (Nikon, Tokyo, Japan) equipped with a color digital camera (DVC 1310C, Austin, Texas, USA). Cell length and diameter were measured manually using the Fiji image analysis software (Rueden *et al.*, 2017). 200 cells in each data set were measured. Cell density was determined by counting the cells with the Fuchs-Rosenthal hemocytometer slide, typically in the fourth day of subcultivation or periodically during the entire period; individual values represent the average of at least six aliquots of every sample. For the fluorescence imaging, Zeiss LSM900 laser scanning microscope (Axio Observer 7, inverted) with Airyscan 2 with Multiplex mode (Carl Zeiss, Jena, Germany) with appropriate filter sets to visualize reporter genes GFP (excitation 488 nm and emission 509 nm wavelengths) and/or mRFP (excitation 590 nm and emission 599 nm wavelengths) was used. Detailed images were obtained with the 40x or 63x water/oil immersion objectives.

**Assays on cell viability, ROS content and PCD**

The trypan blue exclusion test was used to visualize the penetration of the non-viable cells by the dye (van Wees, 2008). Approximately 10 µl of the 0.4 % trypan blue solution (Sigma-Aldrich) was added to the 0.5 ml cell suspension and recorded subsequently. Cell viability was determined as the percentage of dye-negative cells relative to the total number of cells.

For the detection of reactive oxygen species (ROS), the cells were incubated with the 10 µM H2DCFDA (2′,7′-dichlorfluorescein-diacetate; Thermo Fisher Scientific, Waltham, Massachusetts, USA) solution (Akter *et al.*, 2021) for 15 min and washed twice with the BY-2 medium. The relative ROS accumulation is presented as the mean pixel intensity of cells determined by the Zeiss Zen software. In total, about four hundred cells were counted from three independent experiments. The integrity of the vacuoles was determined after 10 min of staining with 10 µM BCECF-AM ((2′,7′-bis-2-carboxyethyl)-5-(and-6) carboxyfluorescein; Sigma-Aldrich; Scheuring *et al.*, 2015). The number of cells with aberrant vacuolar integrity was assessed as a ratio of cells with the cytoplasmic signal to that of the cells showing a normal vacuolar signal. About five hundred cells were processed in three independent experiments. In both cases, the confocal images were acquired with the Plan-Apochromat 10x/0.45 DIC M27 objective.

TUNEL (terminal deoxynucleotidyl transferase dUTP nick end labeling) assay (Tripathi *et al.*, 2017) was performed in 2-day-old cells according to the manufacturer's protocol (TMR red in situ cell death detection kit, Roche Diagnostics GmbH, Heidelberg, Germany) with modifications as described earlier (Smetana *et al.*, 2012). The labeled cells were examined using a color digital camera (DVC 1310C, Austin, Texas, USA) at the Nikon Eclipse E600 microscope. All cells were analyzed from at least 10 view fields, covering approximately 100 cells each. The quantification is expressed as a percentage of cells carrying the TUNEL signal divided by the total cell number in the visual field.

**Auxin uptake assays**

Auxin uptake assays were performed in 3-d-old cells as described earlier (Delbarre *et al.*, 1996; Petrásek *et al.*, 2003). [$^3$H]-2,4-D (10 Ci.mmol$^{-1}$) or [$^3$H]-IAA (25 Ci.mmol$^{-1}$) (American Radiolabeled Chemicals, Inc., St Louis, MO, USA) were added to the equilibrated cell suspension at the beginning of the accumulation assay to the final concentration of 2 nM.

The presented values are means of each triplicate from a representative experiment out of three biological repetitions.

**IAA metabolic profiling**

The harvesting of the 2-d-old BY-2 cells was done 2 hours after the addition of 1 µM IAA into the media, unless stated otherwise. Auxin metabolites were extracted according to previously described procedures (Dobrev & Kamínek, 2002; Dobrev *et al.*, 2023), and determined by the LC-MS quantitative analysis further detailed in Dobrev *et al.* (2023). The samples were processed in triplicates. The results are presented as a mean of at least three independent biological repetitions.

**Transcriptome analysis**

The total RNA was isolated using RNeasy Plant Mini kit (Qiagen, Düsseldorf, Germany) from 50-100 mg of cells cultured in medium for 48 h with IAA added every 12 h, 2 h after the last addition of IAA. Isolated RNA was treated with DNA-Free kit (Thermo Fisher Scientific). RNA purity, concentration and integrity were evaluated on 0.8% agarose gels (v/w) and with the Bioanalyzer RNA Nano 6000 Assay Kit (Agilent Technologies, Santa Clara, CA, USA). RNA sequencing was performed using Illumina NovaSeq 6000 platform. The analysis resulted in at least 15 million 150 bps read pairs. The raw reads were quality-filtered using Rcorrector and Trim Galore scripts (Song & Florea, 2015). Transcript abundances (transcripts per million – TPM) were determined using the Salmon software package (Patro *et al.*, 2017) with parameters --posBias, --seqBias, --gcBias, --numBootstraps 30. The index was built from the *Nicotiana tabacum* v1.0 cDNA dataset (Edwards *et al.*, 2017), by including the *AtPIN5* (*AT5G16530*) gene sequence. Visualization, quality control of data analysis and determination of differentially expressed genes were determined using the sleuth package in R (Love *et al.*, 2014; Pimentel *et al.*, 2017) (version 0.29.0). Transcripts with the q-value <= 0.05 and $\log_2$ fold change >=1 (upregulated) or <= -1 (down-regulated) were considered to be significantly differentially expressed. Other criteria for selection of gene list of interest are specified in corresponding result section.

Gene ontology analysis (statistical overrepresentation test) was done using the Panther Classification System (Mi *et al.*, 2019). Raw sequencing data are available through GEO Series

accession number GSE260945 at the Gene Expression Omnibus (https://www.ncbi.nlm.nih.gov/geo/). The grouping of differentially expressed genes was visualized with the DiVenn software (Sun *et al.*, 2019).


## ACKNOWLEDGEMENTS

We thank Jiří Friml for kindly providing the *Ataxr3-1* construct, Enrico Scarpella for the *PIN5-GFP*$^{MGS}$ lines, Zuzana Vondráková and Nikola Drážná for technical assistance, and Kateřina Malínská for help with image analysis. The work was supported by the Czech Science Foundation (project 19-23773S) to KR, JP and PID. Microscopy was done at the Imaging Facility of the Institute of Experimental Botany and was supported by the Ministry of Education, Youth and Sports of the Czech Republic (LM2023050 Czech-Bioimaging).


## AUTHOR CONTRIBUTIONS

JP and KR conceived the research. JP, KR and MČ designed the experiments. MČ performed most experiments. KM did RT-qPCR and transcriptome analysis. NK and NAS prepared DNA constructs. PS provided preliminary data essential for the initiation of the study. OS performed part of the PCD assays. PID did metabolic profiling. KR, JP and MČ wrote the manuscript. KR acquired funding. All authors have exercised their right to comment on the manuscript.

## CONFLICT OF INTEREST

The authors declare no conflict of interest.

## REFERENCES


**Abdollahi Sisi N, Růžička K**. **2020**. ER-Localized PIN Carriers: Regulators of Intracellular Auxin Homeostasis. *Plants* **9**: 1527.

**Adamowski M, Friml J**. **2015**. PIN-Dependent Auxin Transport: Action, Regulation, and Evolution. *The Plant Cell* **27**: 20–32.

**Akter S, Shahneawz Khan M, N. Smith E, Flashman E**. **2021**. Measuring ROS and redox markers in plant cells. *RSC Chemical Biology* **2**: 1384–1401.

**Andersen CG, Bavnhøj L, Pedersen BP**. **2023**. May the proton motive force be with you: A plant transporter review. *Current Opinion in Structural Biology* **79**: 102535.

**Aoyama T, Chua NH**. **1997**. A glucocorticoid-mediated transcriptional induction system in transgenic plants. *The Plant Journal: For Cell and Molecular Biology* **11**: 605–612.

**Band LR, Wells DM, Larrieu A, Sun J, Middleton AM, French AP, Brunoud G, Sato EM, Wilson MH, Péret B, *et al.* 2012**. Root gravitropism is regulated by a transient lateral auxin gradient controlled by a tipping-point mechanism. *Proceedings of the National Academy of Sciences* **109**: 4668–4673.

**Bandurski RS, Cohen JD, Slovin JP, Reinecke DM**. **1995**. Auxin biosynthesis and metabolism. In: Davies PJ, ed. Plant Hormones. Physiology, Biochemistry and Molecular Biology. Dordrecht: Springer, 39–65.

**Barbez E, Laňková M, Pařezová M, Maizel A, Zažímalová E, Petrášek J, Friml J, Kleine-Vehn J**. **2013**. Single-cell-based system to monitor carrier driven cellular auxin homeostasis. *BMC plant biology* **13**: 20.

**Benková E, Michniewicz M, Sauer M, Teichmann T, Seifertová D, Jürgens G, Friml J**. **2003**. Local, efflux-dependent auxin gradients as a common module for plant organ formation. *Cell* **115**: 591–602.

**Casimiro I, Marchant A, Bhalerao RP, Beeckman T, Dhooge S, Swarup R, Graham N, Inzé D, Sandberg G, Casero PJ, *et al.* 2001**. Auxin transport promotes Arabidopsis lateral root initiation. *The Plant Cell* **13**: 843–852.

**Chen Y, Aung K, Rolčík J, Walicki K, Friml J, Brandizzi F**. **2014a**. Inter-regulation of the unfolded protein response and auxin signaling. *The Plant Journal: For Cell and Molecular Biology* **77**: 97–107.

**Chen C, Letnik I, Hacham Y, Dobrev P, Ben-Daniel B-H, Vanková R, Amir R, Miller G**. **2014b**. ASCORBATE PEROXIDASE6 Protects Arabidopsis Desiccating and Germinating Seeds from Stress and Mediates Cross Talk between Reactive Oxygen Species, Abscisic Acid, and Auxin. *Plant Physiology* **166**: 370–383.

**Chhajed S, Mostafa I, He Y, Abou-Hashem M, El-Domiaty M, Chen S**. **2020**. Glucosinolate Biosynthesis and the Glucosinolate–Myrosinase System in Plant Defense. *Agronomy* **10**: 1786.

**Curtis MD, Grossniklaus U**. **2003**. A gateway cloning vector set for high-throughput functional analysis of genes in planta. *Plant Physiology* **133**: 462–469.

**Delbarre A, Muller P, Imhoff V, Guern J**. **1996**. Comparison of mechanisms controlling uptake and accumulation of 2,4-dichlorophenoxy acetic acid, naphthalene-1-acetic acid, and indole-3-acetic acid in suspension-cultured tobacco cells. *Planta* **198**: 532–541.

**Di Mambro R, Svolacchia N, Dello Ioio R, Pierdonati E, Salvi E, Pedrazzini E, Vitale A, Perilli S, Sozzani R, Benfey PN, *et al.* 2019**. The Lateral Root Cap Acts as an Auxin Sink that Controls Meristem Size. *Current Biology* **29**: 1199-1205.e4.

**Ding Z, Wang B, Moreno I, Dupláková N, Simon S, Carraro N, Reemmer J, Pěnčík A, Chen X, Tejos R, *et al.* 2012**. ER-localized auxin transporter PIN8 regulates auxin homeostasis and male gametophyte development in *Arabidopsis*. *Nature Communications* **3**: 941.

**Dobrev PI, Filepová R, Lacek J, Vondráková Z, Müller K, Maršík P, Drašarová L, Talacko P, Hošek P, Petrášek J**. **2023**. Study of auxin metabolism using stable isotope labeling and LCMS; evidence for in planta auxin decarboxylation pathway. : 2023.06.02.543384.

**Dobrev PI, Kamínek M. 2002**. Fast and efficient separation of cytokinins from auxin and abscisic acid and their purification using mixed-mode solid-phase extraction. *Journal of Chromatography A* **950**: 21–29.

**Edwards KD, Fernandez-Pozo N, Drake-Stowe K, Humphry M, Evans AD, Bombarely A, Allen F, Hurst R, White B, Kernodle SP, *et al.* 2017**. A reference genome for Nicotiana tabacum enables map-based cloning of homeologous loci implicated in nitrogen utilization efficiency. *BMC Genomics* **18**: 448.

**Escamez S, André D, Sztojka B, Bollhöner B, Hall H, Berthet B, Voß U, Lers A, Maizel A, Andersson M, *et al.* 2020**. Cell Death in Cells Overlying Lateral Root Primordia Facilitates Organ Growth in Arabidopsis. *Current Biology* **30**: 455-464.e7.

**Escamez S, Tuominen H. 2014**. Programmes of cell death and autolysis in tracheary elements: when a suicidal cell arranges its own corpse removal. *Journal of Experimental Botany* **65**: 1313–1321.

**Fahey JW, Zalcmann AT, Talalay P. 2001**. The chemical diversity and distribution of glucosinolates and isothiocyanates among plants. *Phytochemistry* **56**: 5–51.

**Friml J, Wiśniewska J, Benková E, Mendgen K, Palme K. 2002**. Lateral relocation of auxin efflux regulator PIN3 mediates tropism in Arabidopsis. *Nature* **415**: 806–809.

**Fukuda H, Komamine A. 1980**. Establishment of an Experimental System for the Study of Tracheary Element Differentiation from Single Cells Isolated from the Mesophyll of Zinnia elegans. *Plant Physiology* **65**: 57–60.

**Gälweiler L, Guan C, Müller A, Wisman E, Mendgen K, Yephremov A, Palme K. 1998**. Regulation of polar auxin transport by AtPIN1 in Arabidopsis vascular tissue. *Science (New York, N.Y.)* **282**: 2226–2230.

**Hayashi K, Arai K, Aoi Y, Tanaka Y, Hira H, Guo R, Hu Y, Ge C, Zhao Y, Kasahara H, *et al.* 2021**. The main oxidative inactivation pathway of the plant hormone auxin. *Nature Communications* **12**: 6752.

**Hrnčiřík K, Valušek J, Velíšek J. 1998**. A study on the formation and stability of ascorbigen in an aqueous system. *Food Chemistry* **63**: 349–355.

**Kacprzyk J, Burke R, Schwarze J, McCabe PF. 2022**. Plant programmed cell death meets auxin signalling. *The FEBS Journal* **289**: 1731–1745.

**Katz E, Chamovitz DA. 2017**. Wounding of Arabidopsis leaves induces indole-3-carbinol-dependent autophagy in roots of Arabidopsis thaliana. *The Plant Journal: For Cell and Molecular Biology* **91**: 779–787.

**Katz E, Nisani S, Yadav BS, Woldemariam MG, Shai B, Obolski U, Ehrlich M, Shani E, Jander G, Chamovitz DA. 2015**. The glucosinolate breakdown product indole-3-carbinol acts as an auxin antagonist in roots of Arabidopsis thaliana. *The Plant Journal* **82**: 547–555.

**Kerchev P, Mühlenbock P, Denecker J, Morreel K, Hoeberichts FA, Van Der Kelen K, Vandorpe M, Nguyen L, Audenaert D, Van Breusegem F. 2013**. Activation of auxin signalling counteracts photorespiratory H2O2-dependent cell death. *Plant, Cell & Environment* **38**: 253–265.

**Kerk NM, Jiang K, Feldman LJ. 2000**. Auxin Metabolism in the Root Apical Meristem. *Plant Physiology* **122**: 925–932.

**Knox K, Grierson CS, Leyser O**. **2003**. AXR3 and SHY2 interact to regulate root hair development. *Development (Cambridge, England)* **130**: 5769–5777.

**Kubo M, Udagawa M, Nishikubo N, Horiguchi G, Yamaguchi M, Ito J, Mimura T, Fukuda H, Demura T**. **2005**. Transcription switches for protoxylem and metaxylem vessel formation. *Genes & Development* **19**: 1855–1860.

**Leyser HMO, Pickett FB, Dharmasiri S, Estelle M**. **1996**. Mutations in the AXR3 gene of Arabidopsis result in altered auxin response including ectopic expression from the SAUR-AC1 promoter. *The Plant Journal* **10**: 403–413.

**Love MI, Huber W, Anders S**. **2014**. Moderated estimation of fold change and dispersion for RNA-seq data with DESeq2. *Genome Biology* **15**: 550.

**Ludwig-Müller J, Jülke S, Bierfreund NM, Decker EL, Reski R**. **2009**. Moss (Physcomitrella patens) GH3 proteins act in auxin homeostasis. *New Phytologist* **181**: 323–338.

**Mi H, Muruganujan A, Ebert D, Huang X, Thomas PD**. **2019**. PANTHER version 14: More genomes, a new PANTHER GO-slim and improvements in enrichment analysis tools. *Nucleic Acids Research* **47**: D419–D426.

**Mitchison GJ**. **1980**. A Model for Vein Formation in Higher Plants. *Proceedings of the Royal Society of London. Series B, Biological Sciences* **207**: 79–109.

**Mravec J, Kubeš M, Bielach A, Gaykova V, Petrášek J, Skůpa P, Chand S, Benková E, Zažímalová E, Friml J**. **2008**. Interaction of PIN and PGP transport mechanisms in auxin distribution-dependent development. *Development* **135**: 3345–3354.

**Mravec J, Skůpa P, Bailly A, Hoyerová K, Krecek P, Bielach A, Petrásek J, Zhang J, Gaykova V, Stierhof Y-D, *et al.* 2009**. Subcellular homeostasis of phytohormone auxin is mediated by the ER-localized PIN5 transporter. *Nature* **459**: 1136–1140.

**Müller K, Dobrev PI, Pěnčík A, Hošek P, Vondráková Z, Filepová R, Malínská K, Brunoni F, Helusová L, Moravec T, *et al.* 2021**. DIOXYGENASE FOR AUXIN OXIDATION 1 catalyzes the oxidation of IAA amino acid conjugates. *Plant Physiology* **187**: 103–115.

**Müller K, Hošek P, Laňková M, Vosolsobě S, Malínská K, Čarná M, Fílová M, Dobrev PI, Helusová M, Hoyerová K, *et al.* 2019**. Transcription of specific auxin efflux and influx carriers drives auxin homeostasis in tobacco cells. *The Plant Journal: For Cell and Molecular Biology* **100**: 627–640.

**Nagata T, Nemoto Y, Hasezawa S**. **1992**. Tobacco BY-2 Cell Line as the "HeLa" Cell in the Cell Biology of Higher Plants. In: Jeon KW, Friedlander M, eds. International Review of Cytology. Academic Press, 1–30.

**Nishimura T, Nakano H, Hayashi K, Niwa C, Koshiba T**. **2009**. Differential downward stream of auxin synthesized at the tip has a key role in gravitropic curvature via TIR1/AFBs-mediated auxin signaling pathways. *Plant & Cell Physiology* **50**: 1874–1885.

**Ostrowski M, Świdziński M, Ciarkowska A, Jakubowska A**. **2014**. IAA–amido synthetase activity and GH3 expression during development of pea seedlings. *Acta Physiologiae Plantarum* **36**: 3029–3037.

**Ottenschläger I, Wolff P, Wolverton C, Bhalerao RP, Sandberg G, Ishikawa H, Evans M, Palme K**. **2003**. Gravity-regulated differential auxin transport from columella to lateral root cap cells. *Proceedings of the National Academy of Sciences* **100**: 2987–2991.

**Patro R, Duggal G, Love MI, Irizarry RA, Kingsford C**. **2017**. Salmon provides fast and bias-aware quantification of transcript expression. *Nature Methods* **14**: 417–419.

**Peñarrubia L, Romero P, Carrió-Seguí A, Andrés-Bordería A, Moreno J, Sanz A**. **2015**. Temporal aspects of copper homeostasis and its crosstalk with hormones. *Frontiers in Plant Science* **6**: 255.

**Petrásek J, Cerná A, Schwarzerová K, Elckner M, Morris DA, Zazímalová E**. **2003**. Do phytotropins inhibit auxin efflux by impairing vesicle traffic? *Plant Physiology* **131**: 254–263.

**Petrasek J, Mravec J, Bouchard R, Blakeslee JJ, Abas M, Seifertová D, Wisniewska J, Tadele Z, Kubes M, Covanová M, *et al.* 2006**. PIN proteins perform a rate-limiting function in cellular auxin efflux. *Science (New York, N.Y.)* **312**: 914–918.

**Petrášek J, Zazímalová E**. **2006**. The BY-2 Cell Line as a Tool to Study Auxin Transport. In: Nagata T, Matsuoka K, Inzé D, eds. Biotechnology in Agriculture and Forestry. Tobacco BY-2 Cells: From Cellular Dynamics to Omics. Berlin, Heidelberg: Springer Science & Business Media, 107–118.

**Petrov V, Hille J, Mueller-Roeber B, Gechev TS**. **2015**. ROS-mediated abiotic stress-induced programmed cell death in plants. *Frontiers in Plant Science* **6**.

**Pimentel H, Bray NL, Puente S, Melsted P, Pachter L**. **2017**. Differential analysis of RNA-seq incorporating quantification uncertainty. *Nature Methods* **14**: 687–690.

**Rakusová H, Gallego-Bartolomé J, Vanstraelen M, Robert HS, Alabadí D, Blázquez MA, Benková E, Friml J**. **2011**. Polarization of PIN3-dependent auxin transport for hypocotyl gravitropic response in Arabidopsis thaliana. *The Plant Journal* **67**: 817–826.

**Raven JA**. **1975**. Transport of indoleacetic acid in plant cells in relation to pH and electrical potential gradients, and its significance for polar IAA transport. *New Phytologist* **74**: 163–172.

**Ravichandran SJ, Linh NM, Scarpella E**. **2020**. The canalization hypothesis – challenges and alternatives. *New Phytologist* **227**: 1051–1059.

**Reinhardt D, Pesce E-R, Stieger P, Mandel T, Baltensperger K, Bennett M, Traas J, Friml J, Kuhlemeier C**. **2003**. Regulation of phyllotaxis by polar auxin transport. *Nature* **426**: 255–260.

**Rolland-Lagan A-G, Prusinkiewicz P**. **2005**. Reviewing models of auxin canalization in the context of leaf vein pattern formation in Arabidopsis. *The Plant Journal* **44**: 854–865.

**Rubery PH, Sheldrake AR**. **1974**. Carrier-mediated auxin transport. *Planta* **118**: 101–121.

**Rueden CT, Schindelin J, Hiner MC, DeZonia BE, Walter AE, Arena ET, Eliceiri KW**. **2017**. ImageJ2: ImageJ for the next generation of scientific image data. *BMC Bioinformatics* **18**: 529.

**Ruzicka K, Ursache R, Hejátko J, Helariutta Y**. **2015**. Xylem development – from the cradle to the grave. *New Phytologist* **207**: 519–535.

**Sachs T**. **1991**. Cell polarity and tissue patterning in plants. *Development* **113**: 83–93.

**Scheuring D, Schöller M, Kleine-Vehn J, Löfke C. 2015**. Vacuolar Staining Methods in Plant Cells. In: Estevez JM, ed. Methods in Molecular Biology. Plant Cell Expansion: Methods and Protocols. New York, NY: Springer, 83–92.

**Seifertová D, Skůpa P, Rychtář J, Laňková M, Pařezová M, Dobrev PI, Hoyerová K, Petrášek J, Zažímalová E. 2014**. Characterization of transmembrane auxin transport in Arabidopsis suspension-cultured cells. *Journal of Plant Physiology* **171**: 429–437.

**Sheldrake AR. 2021**. The production of auxin by dying cells. *Journal of Experimental Botany* **72**: 2288–2300.

**Simon S, Kubeš M, Baster P, Robert S, Dobrev PI, Friml J, Petrášek J, Zažímalová E. 2013**. Defining the selectivity of processes along the auxin response chain: a study using auxin analogues. *New Phytologist* **200**: 1034–1048.

**Smetana O, Široký J, Houlné G, Opatrný Z, Chabouté M-E. 2012**. Non-apoptotic programmed cell death with paraptotic-like features in bleomycin-treated plant cells is suppressed by inhibition of ATM/ATR pathways or NtE2F overexpression. *Journal of Experimental Botany* **63**: 2631–2644.

**Song L, Florea L. 2015**. Rcorrector: efficient and accurate error correction for Illumina RNA-seq reads. *GigaScience* **4**: s13742-015-0089-y.

**Su N, Zhu A, Tao X, Ding ZJ, Chang S, Ye F, Zhang Y, Zhao C, Chen Q, Wang J, *et al.* 2022**. Structures and mechanisms of the Arabidopsis auxin transporter PIN3. *Nature* **609**: 616–621.

**Sun L, Dong S, Ge Y, Fonseca JP, Robinson ZT, Mysore KS, Mehta P. 2019**. DiVenn: An Interactive and Integrated Web-Based Visualization Tool for Comparing Gene Lists. *Frontiers in Genetics* **10**: 421.

**Swarup K, Benková E, Swarup R, Casimiro I, Péret B, Yang Y, Parry G, Nielsen E, De Smet I, Vanneste S, *et al.* 2008**. The auxin influx carrier LAX3 promotes lateral root emergence. *Nature Cell Biology* **10**: 946–954.

**Tognetti VB, Mühlenbock P, Van Breusegem F. 2012**. Stress homeostasis – the redox and auxin perspective. *Plant, Cell & Environment* **35**: 321–333.

**Tripathi AK, Pareek A, Singla-Pareek SL. 2017**. TUNEL Assay to Assess Extent of DNA Fragmentation and Programmed Cell Death in Root Cells under Various Stress Conditions. *Bio-Protocol* **7**: e2502.

**Ung KL, Schulz L, Kleine-Vehn J, Pedersen BP, Hammes UZ. 2023a**. Auxin transport at the endoplasmic reticulum: roles and structural similarity of PIN-FORMED and PIN-LIKES. *Journal of Experimental Botany*: erad192.

**Ung KL, Schulz L, Stokes DL, Hammes UZ, Pedersen BP. 2023b**. Substrate recognition and transport mechanism of the PIN-FORMED auxin exporters. *Trends in Biochemical Sciences*.

**Ung KL, Winkler M, Schulz L, Kolb M, Janacek DP, Dedic E, Stokes DL, Hammes UZ, Pedersen BP. 2022**. Structures and mechanism of the plant PIN-FORMED auxin transporter. *Nature* **609**: 605–610.

**Valandro F, Menguer PK, Cabreira-Cagliari C, Margis-Pinheiro M, Cagliari A. 2020**. Programmed cell death (PCD) control in plants: New insights from the Arabidopsis thaliana deathosome. *Plant Science* **299**: 110603.

**Van Durme M, Nowack MK**. **2016**. Mechanisms of developmentally controlled cell death in plants. *Current Opinion in Plant Biology* **29**: 29–37.

**Verna C, Sawchuk MG, Linh NM, Scarpella E**. **2015**. Control of vein network topology by auxin transport. *BMC Biology* **13**: 94.

**van Wees S**. **2008**. Phenotypic analysis of Arabidopsis mutants: trypan blue stain for fungi, oomycetes, and dead plant cells. *CSH protocols* **2008**: pdb.prot4982.

**Weijers D, Ljung K, Leyser O**. **2021**. *Auxin Signaling: From Synthesis to Systems Biology, Second Edition*. Cold Spring Harbor Laboratory Press.

**Winicur ZM, Zhang GF, Staehelin LA**. **1998**. Auxin deprivation induces synchronous Golgi differentiation in suspension-cultured tobacco BY-2 cells. *Plant Physiology* **117**: 501–513.

**Xuan W, Audenaert D, Parizot B, Möller BK, Njo MF, De Rybel B, De Rop G, Van Isterdael G, Mähönen AP, Vanneste S, *et al.* 2015**. Root Cap-Derived Auxin Pre-patterns the Longitudinal Axis of the Arabidopsis Root. *Current Biology* **25**: 1381–1388.

**Xuan W, Band LR, Kumpf RP, Damme DV, Parizot B, Rop GD, Opdenacker D, Möller BK, Skorzinski N, Njo MF, *et al.* 2016**. Cyclic programmed cell death stimulates hormone signaling and root development in Arabidopsis. *Science* **351**: 384–387.

**Yang Z, Xia J, Hong J, Zhang C, Wei H, Ying W, Sun C, Sun L, Mao Y, Gao Y, *et al.* 2022**. Structural insights into auxin recognition and efflux by Arabidopsis PIN1. *Nature* **609**: 611–615.

**Zou W, Lin P, Zhao Z, Wang D, Qin L, Xu F, Su Y, Wu Q, Que Y**. **2022**. Genome-Wide Identification of Auxin-Responsive GH3 Gene Family in Saccharum and the Expression of ScGH3-1 in Stress Response. *International Journal of Molecular Sciences* **23**: 12750.

**Zuo J, Niu QW, Chua NH**. **2000**. Technical advance: An estrogen receptor-based transactivator XVE mediates highly inducible gene expression in transgenic plants. *The Plant Journal: For Cell and Molecular Biology* **24**: 265–273.

**FIGURE LEGENDS**

**Figure 1.** The hallmarks of auxin starvation in tobacco BY-2 cell cultures. (a, b) The induction of the *XVE::AtPIN7* transgene leads to increased cell elongation (a) and decreased growth, monitored by the cell density in the media (b). (c-e) The induction of *XVE::Ataxr3-1* phenocopies auxin starvation phenotypes, documented by representative image on (c), quantification of reduced proliferation (d) and increased cell elongation ($P < 0.001$ by Student's *t*-test) (e). (f) The cell density of the wild-type BY-2 cells decreases with the growing concentration of supplied PEO-IAA, an inhibitor of auxin-dependent gene expression ($F(5,48) = [11.112]$, $P < 0.001$ by one-way ANOVA). On the dot plots, the open symbols are averages ± S.E. $^{**}P < 0.01$, $^{***}P < 0.001$ by Student's *t*-test. Scale bars: 50 µm.

**Figure 2.** The conditional expression of *XVE::AtPIN5* in BY-2 cells mimics the auxin starvation phenotypes. (a-c) The induction of *XVE::AtPIN5* in the cell line cultured in a standard medium with 2,4-D leads to increased cell elongation (a), plotted on (b, $P < 0.05$ by Student's *t*-test), and reduced proliferation rate (c). (d, e) The induction of *XVE::AtPIN5-GFP* in the cells co-expressing auxin *DR5::RFP* reporter results in co-localization of PIN5-GFP with the ER-targeted RFP (d) and lowering the RFP expression in a reduction of the fluorescence in cells in the upper-intensity quantiles (e). Scale bars: 50 µm. On (c), the open symbols are averages ± S.E. On (e), the vertical error bars represent median ± 95% confidence intervals. $^{***}P < 0.001$ by Student's *t*-test.

**Figure 3.** Replacing 2,4-D with the native auxin IAA in media enhances the auxin starvation effects caused by the induction of *XVE::AtPIN5*. (a) The comparison of the cell proportions of the control *XVE::AtPIN5* cells cultivated in the medium supplemented with 2,4-D or IAA reveals the increase of the elongation growth in the presence of IAA ($P < 0.001$ by Student's *t*-test). (b-c) The cell proliferation rate of cells containing the induced *XVE::AtPIN5* transgene is even lower in the medium with IAA added at the beginning of subcultivation, the representative image on (b), the corresponding quantification of cell density on (c). (d, e) The phenotype of the *XVE::AtPIN5* cells cultured in a medium continuously supplemented with IAA every 12 hours during the monitored cultivation period leads to the partial reversion of the starvation phenotypes in the control lines, however, the induction of the transgene leads to strong auxin starvation phenotypes, as documented at the representative

image on (d) and by the quantification of the cell growth on (e). (f, g) The induction of *XVE::AtPIN5* results in higher uptake of [$^3$H]-IAA (f), but shows no effect on uptake of [$^3$H]-2,4-D (g). Scale bars: 50 µm. On the bar plots, the open symbols are averages ± S.E. $^{**}P < 0.01$, $^{***}P < 0.001$ by Student's *t*-test.

**Figure 4.** An increased incidence of symptoms of PCD following induction of *XVE::AtPIN5*. (a-b) The replacement of 2,4-D with IAA leads to more frequent cytoplasm shrinkage and hereafter increased accumulation of the trypan blue dye inside cells (arrowheads), where *XVE::AtPIN5* was induced, as documented by representative images on (a) and the inverse frequency of the trypan-blue intracellular staining on (b). (c) DiVenn diagram shows that a large part of differentially expressed genes following the *XVE::AtPIN5* induction is shared with those from the cultures undergoing auxin starvation; red, significantly upregulated genes; blue, downregulated genes; yellow, opposite expression changes. A single dot denotes a group of 10 genes. (d, e) An increased fluorescence intensity on confocal images of the H2DCFDA staining of *XVE::AtPIN5* lines detects the elevated presence of reactive oxygen species (ROS) following the transgene induction (d), as quantified in (e). (f, g) Confocal images of cells stained by BCECF-AM to label acidic areas (f), as quantified in (g), document that the *XVE::AtPIN5* induction leads to decreased acidity in vacuoles but increased acidity in the cytoplasm and nucleus area (arrowheads). (h, i) Confocal images of TUNEL staining, marking the disintegration of nuclear DNA (red channel: TUNEL, blue channel: nuclear DAPI staining) (h), shows an enhanced labeling frequency in the cells where the *XVE::AtPIN5* construct was induced (i). For (d) and (f), the color intensity is indicated by the rainbow color lookup table (inset on (d)). Scale bars: 50 µm. On the dot plots, the open symbols are averages ± S.E. $^{*}P < 0.05$, $^{**}P < 0.01$, $^{***}P < 0.001$ by Student's *t*-test.

**Figure 5.** Inducible *XVE::AtPIN5* expression in BY-2 cells promotes IAA deactivation by the decarboxylation pathway. (a) A scheme of current understanding of main IAA degradation pathways (products of IAA oxidation pathway in blue, products of IAA decarboxylation in red). (b) LC-MS quantification of IAA and its metabolites in the cells expressing *XVE::AtPIN5* cultured on the standard 2,4-D-supplemented media shows moderately decreased levels of IAA and its most degradation products. (c) The induction of *XVE::AtPIN5* in the cells cultivated in media supplemented with IAA added every 12 hours leads to a dramatic drop of

IAA and its conjugates, while the compounds belonging to the IAA decarboxylation pathway show steadily elevated levels. On (b) and (c), the open symbols indicate the mean from three independent measurements; the bars are ± S.E. *$P$ < 0.05, **$P$ < 0.01, ***$P$ < 0.001, by Student's $t$-test, n. s.: not significant at $\alpha_{0.05}$. IAA: indole-3-acetic acid, IAA-Asp: IAA-aspartate, IAA-GE: IAA-glucose ester, OxIAA-Asp: Oxo-IAA-aspartate, Abg: ascorbigen, DiHAbg: dihydroascorbigen, I3M: indole-3-methylglutathione. The cells were harvested 2 hours after the addition of 1 µM IAA.

**Figure 6.** The indole-3-carbinol treatment leads to growth arrest and reduced viability of BY-2 cells. (a) The exposure of BY-2 cells to 50 µM I3C in the media leads to increased cell expansion in diameter ($P$ < 0.001 by Student's $t$-test) and (b) decreased proliferation, monitored by the cell density in the media and cell viability. (c-d) The I3C-treated cells show also and increased incidence of dead cells visualized by trypan blue staining, representative images on (c), quantified on (d). Scale bars: 50 µm. On the dot plots, the open symbols are averages ± S.E. ***$P$ < 0.001 by Student's $t$-test.

**SUPPLEMENTAL FIGURE LEGENDS**

**Figure S1.** The additional features of auxin starvation of tobacco BY-2 cells. (a) The induction of the *GVG::AtPIN7* transgene leads to decreased cell density, reflecting their low proliferation rate during the whole subcultivation interval. (b) The enhanced cell expansion is typical for cultivation on the auxin-free medium (shown on the *GVG::AtPIN7* line without the chemical inducer). On (a), the open symbols are averages ± S.E. Scale bars: 50 µm.

**Figure S2.** The conditional expression of *GVG::AtPIN5* in the BY-2 cells mimics the auxin starvation phenotypes. (a-c) The induction of *GVG::AtPIN5* in the cell line cultured in standard medium with 2,4-D leads to increased cell expansion ($P$ < 0.001 by Student's t-test) and reduced proliferation rates (c). On (c), the open symbols are averages ± S.E. Scale bars: 50 µm.

**Figure S3.** The pattern and intensity of the AtPIN5-GFP foci are comparable in both standard 2,4-D-containing medium and that continuously supplemented with IAA every 12 hours. The signal intensity is indicated by the green fire blue rainbow lookup table. Scale bars: 10 µm.

**Figure S4.** Increased frequency of symptoms of PCD and its relationship to auxin starvation following induction of *AtPIN5*. (a, b) The representative images of incorporation of the trypan blue inside the cells following induction of *GVG::AtPIN5* (a), quantified on (b). (c, d) Quality control of RNA-Seq data processing, a heat-map representing Jensen-Shannon divergence between individual samples (sorted by internal sample IDs) (c), projections of individual samples onto the principal components (PC) (d). (e) An increased fluorescence on confocal images of the *GVG::AtPIN5* cells stained by 10 µM H2DCFDA to detect reactive oxygen species (ROS), following the transgene induction. (f) TUNEL staining (left: TUNEL, middle: control nuclear DAPI staining, right: merged false-colored images) marks an enhanced disintegration of nuclear DNA in the cells where *GVG::AtPIN5* was induced. On (b), the box plot of a data set of 2000 cells in total, error bars represent SE, ***$P < 0.001$ by Student's *t*-test. Scale bars: 50 µm.

**Figure S5.** Additional experiments corroborating the role of the IAA decarboxylation pathway following the *AtPIN5* expression. (a) Representative LC-MS analysis of IAA and its metabolites in cells expressing *XVE::AtPIN5* determined immediately after 1 µM IAA supply ($t_0$). While the exogenously applied IAA is absorbed immediately, the levels of its metabolites are still barely detectable. (b) LC-MS analysis of IAA and its metabolites in cells expressing *GVG::AtPIN5* cultured on the standard 2,4-D-supplemented media, 2 hours after adding 1 µM IAA. The induction of *GVG::AtPIN5* leads to the increase of the IAA conjugate content. Open symbols indicate the mean of three technical measurements; the bars are ± S.E. **$P < 0.01$, ***$P < 0.001$ by Student's *t*-test, n. s.: not significant at $\alpha_{0.05}$. IAA: indole-3-acetic acid, IAA-Asp: IAA-aspartate, IAA-GE: IAA-glucose ester, IAA-Glu: IAA-glutamate, Abg: ascorbigen, I3C: indole-3-carbinol.

**Table S1.** Results of PANTHER Overrepresentation test (GO - Molecular function) of transcripts significantly upregulated in both auxin-starved and the *XVE::AtPIN5*-expressing cells.

**Table S2.** Results of PANTHER Overrepresentation test (GO - Molecular function) of transcripts significantly upregulated in BY-2 cells carrying induced *XVE::AtPIN5*, compared to untreated controls and auxin-starved cells.

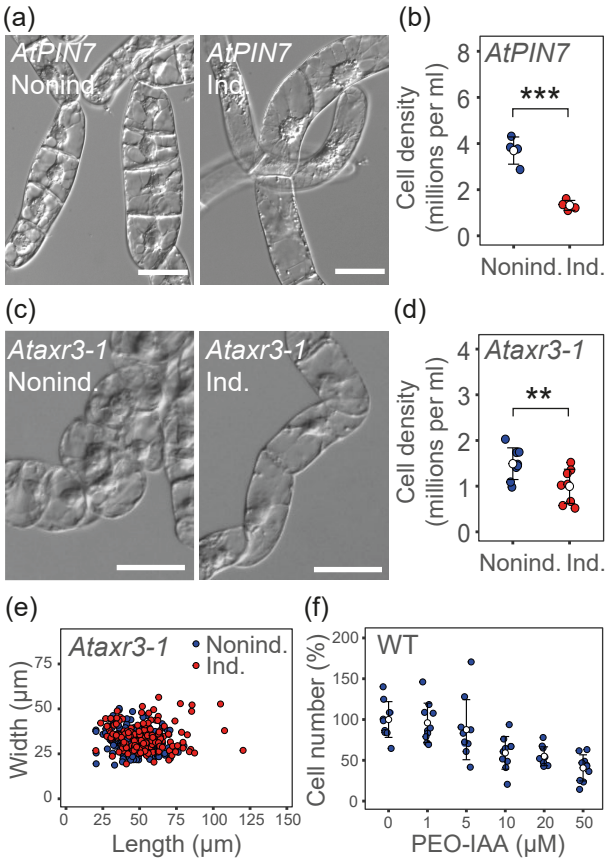
(a)
AtPIN7
Nonind.
AtPIN7
Ind.
(b)
AtPIN7
***
Cell density (millions per ml)
0
2
4
6
8
Nonind.
Ind.
(c)
Ataxr3-1
Nonind.
Ataxr3-1
Ind.
(d)
Ataxr3-1
**
Cell density (millions per ml)
0
1
2
3
4
Nonind.
Ind.
(e)
Ataxr3-1
Nonind.
Ind.
Width (µm)
0
25
50
75
0
25
50
75
100
125
150
Length (µm)
(f)
WT
Cell number (%)
0
50
100
150
200
0
1
5
10
20
50
PEO-IAA (µM)

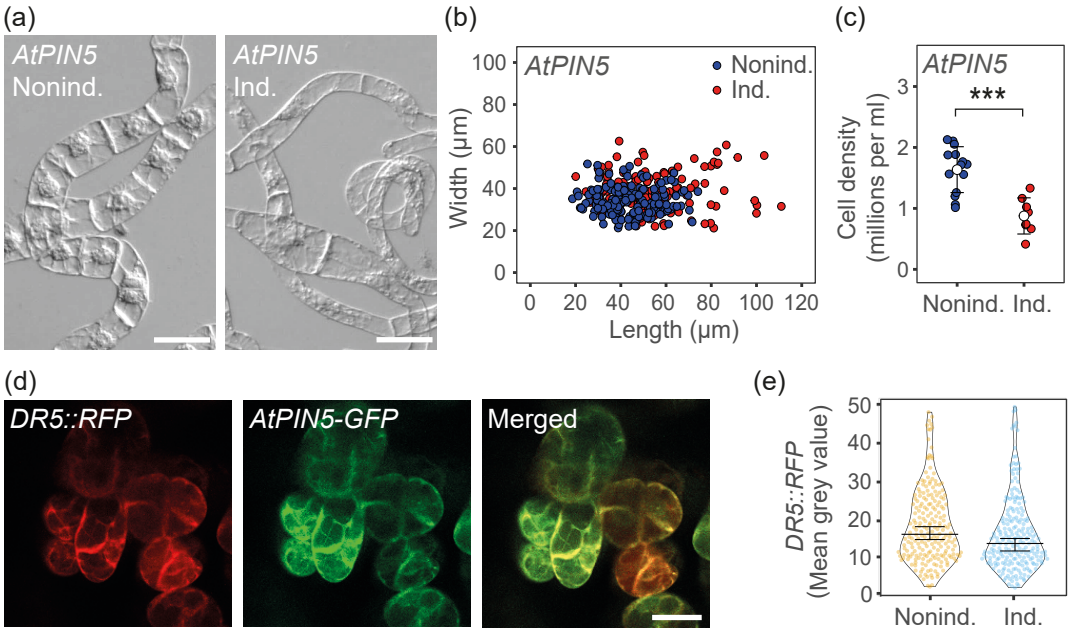
(a)
AtPIN5
Nonind.
AtPIN5
Ind.
(b)
AtPIN5
Nonind.
Ind.
Width (µm)
Length (µm)
(c)
AtPIN5
***
Cell density
(millions per ml)
Nonind.
Ind.
(d)
DR5::RFP
AtPIN5-GFP
Merged
(e)
DR5::RFP
(Mean grey value)
Nonind.
Ind.

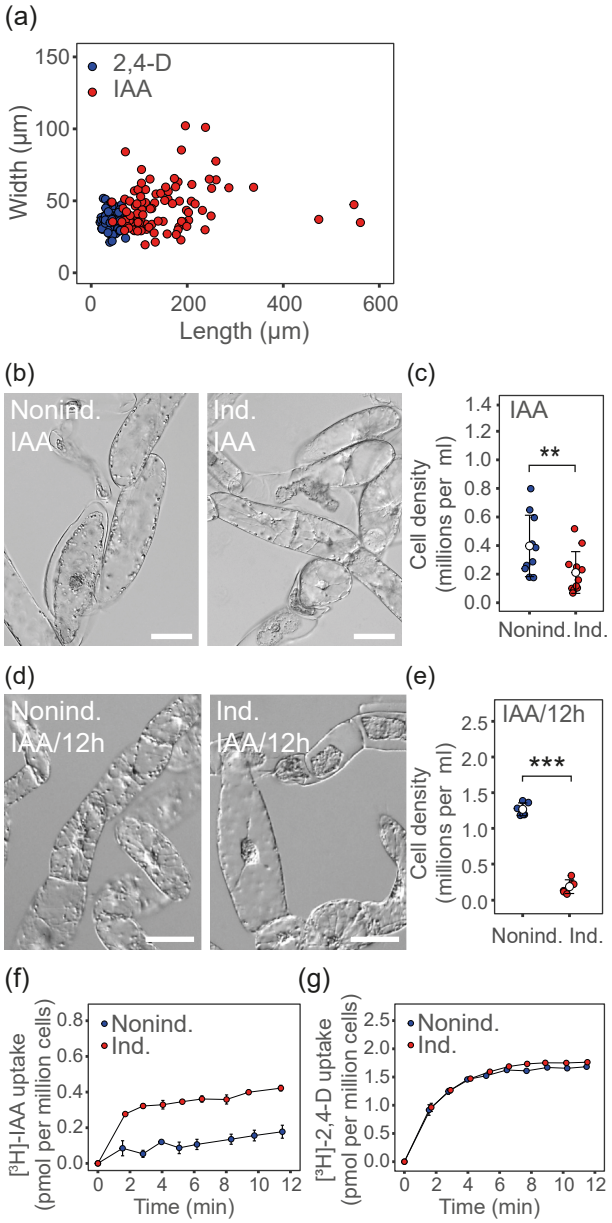
(a)
2,4-D
IAA
Width (µm)
Length (µm)
(b)
Nonind.
IAA
Ind.
IAA
(c)
IAA
Cell density
(millions per ml)
Nonind.
Ind.
(d)
Nonind.
IAA/12h
Ind.
IAA/12h
(e)
IAA/12h
Cell density
(millions per ml)
Nonind.
Ind.
(f)
Nonind.
Ind.
[³H]-IAA uptake
(pmol per million cells)
Time (min)
(g)
Nonind.
Ind.
[³H]-2,4-D uptake
(pmol per million cells)
Time (min)

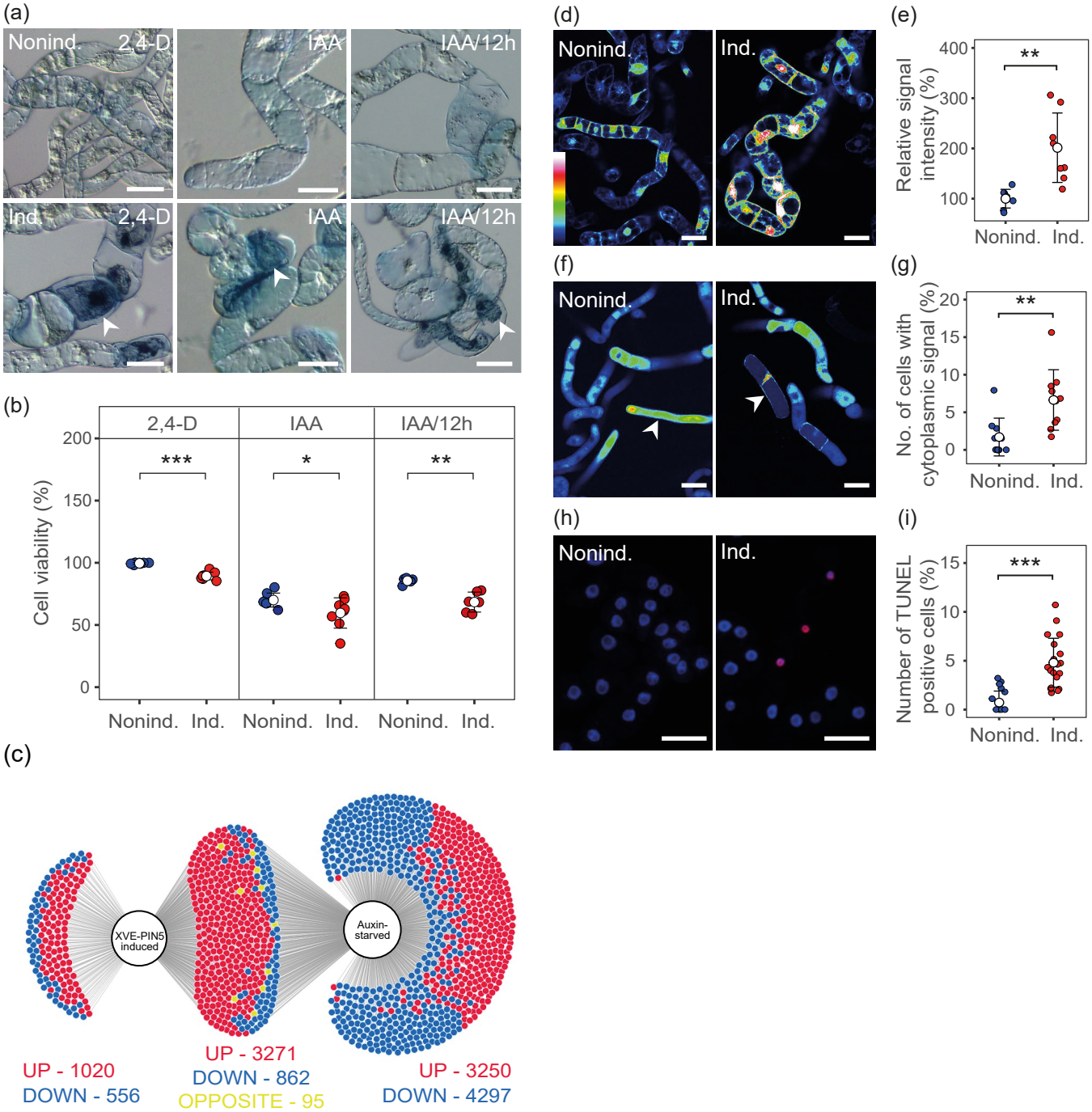
(a)
Nonind.
2,4-D
IAA
IAA/12h
Ind.
2,4-D
IAA
IAA/12h
(b)
2,4-D
IAA
IAA/12h
Cell viability (%)
200
150
100
50
0
***
*
**
Nonind.
Ind.
Nonind.
Ind.
Nonind.
Ind.
(c)
XVE-PIN5 induced
Auxin-starved
UP - 1020
DOWN - 556
UP - 3271
DOWN - 862
OPPOSITE - 95
UP - 3250
DOWN - 4297
(d)
Nonind.
Ind.
(e)
Relative signal intensity (%)
400
300
200
100
**
Nonind.
Ind.
(f)
Nonind.
Ind.
(g)
No. of cells with cytoplasmic signal (%)
20
15
10
5
0
**
Nonind.
Ind.
(h)
Nonind.
Ind.
(i)
Number of TUNEL positive cells (%)
15
10
5
0
***
Nonind.
Ind.

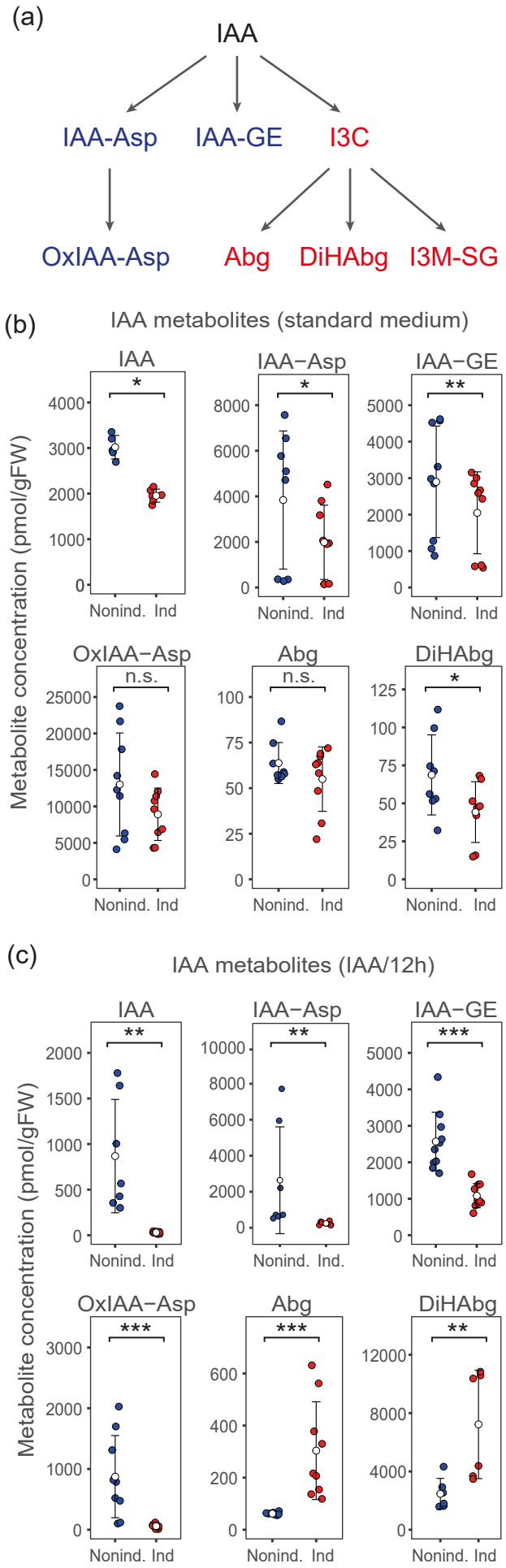
(a)
IAA
IAA-Asp
IAA-GE
I3C
OxIAA-Asp
Abg
DiHAbg
I3M-SG
(b)
IAA metabolites (standard medium)
Metabolite concentration (pmol/gFW)
IAA
IAA−Asp
IAA−GE
OxIAA−Asp
Abg
DiHAbg
Nonind.
Ind
n.s.
(c)
IAA metabolites (IAA/12h)
Metabolite concentration (pmol/gFW)
IAA
IAA−Asp
IAA−GE
OxIAA−Asp
Abg
DiHAbg
Nonind.
Ind.

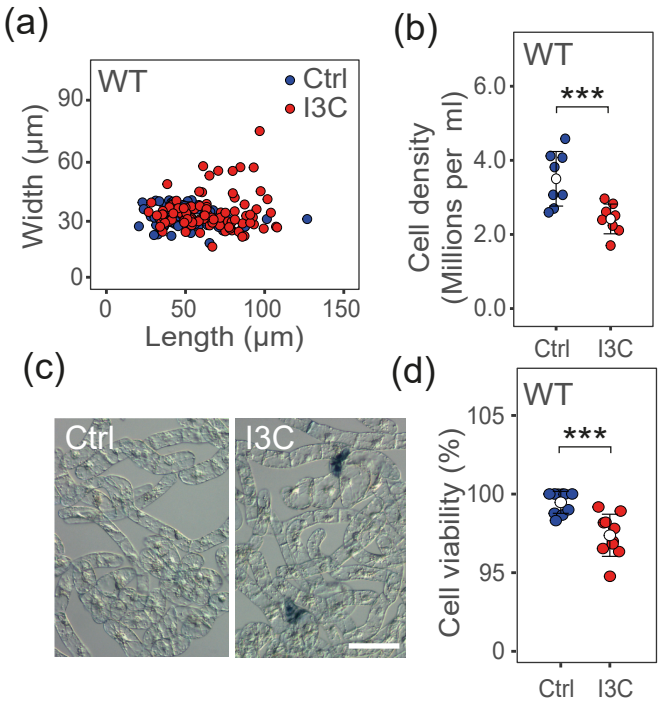
(a)
WT
Ctrl
I3C
Width (μm)
Length (μm)
0
30
60
90
0
50
100
150
(b)
WT
***
Cell density
(Millions per ml)
0.0
2.0
4.0
6.0
Ctrl
I3C
(c)
Ctrl
I3C
(d)
WT
***
Cell viability (%)
0
95
100
105
Ctrl
I3C